Supplementary Information

Impact of atmospheric water vapor on the thermal decomposition of calcium hydroxide: A universal kinetic approach to a physico-geometrical consecutive reaction in solid–gas systems under different partial pressures of product gas

Nobuyoshi Koga,[1,*] Loic Favergeon,[2] and Satoki Kodani[1]
[1]Department of Science Education, Graduate School of Education, Hiroshima University, 1-1-1 Kagamiyama, Higashi-Hiroshima 739-8524, Japan
[2] Mines Saint-Etienne, University of Lyon, CNRS, UMR 5307 LGF, Centre SPIN, F-42023 Saint-Etienne, France

Contents

* Corresponding Author. Tel/Fax: + 81-82-424-7092, e-mail: nkoga@hiroshima-u.ac.jp

S1. Experimental setup and calibration of instruments

A humidity control TG–DTA system (Thermoplus TG-DTA/HUM-1, Rigaku) was used for measuring the mass-loss curves for the thermal decomposition of $Ca(OH)_2$ under controlled $p(H_2O)$ conditions. The measurement system was composed of a TG–DTA instrument (TG-8120, Rigaku) with an electric furnace surrounded by a water circulating pipe, a humidity controller (HUM-1, Rigaku), and a water circulator with a temperature controller (F 25, Julabo).

The TG–DTA instrument was preliminarily calibrated in relation to mass changes and temperature. Calibration with respect to changes in mass was performed at room temperature by the addition/removal of a 10 mg standard weight to/from the sample holder. Subsequently, the accuracy of the mass-change values at high temperatures was confirmed by measuring mass changes associated with the thermal decomposition of a calcium oxalate monohydrate sample (>99.9985%, Alfa Aesar) at three different $p(H_2O)$ values, i.e., 0.65, 1.85, and 5.65 kPa.

Temperature calibration of the TG–DTA instrument was also carried out under the aforementioned $p(H_2O)$ values. The onset temperature of the DTA endothermic peak recorded for the melting of pure metals (In, Sn, Pb, Zn, Al, and Ag, >99.99%, Nilaco) was calibrated in reference to the melting point reported in literature. An empty platinum pan was used as a reference and a counterbalance for the TG–DTA measurements to avoid any possible absorption/desorption of water vapor on the reference.

Wet N_2 gas with a controlled $p(H_2O)$ value was generated by mixing dry N_2 gas and wet N_2 gas produced by bubbling N_2 in a water bath heated at a specific temperature within the range of 298–333 K while using a humidity controller (HUM-1, Rigaku). The mixed "wet" gas was transferred to the forefront of the furnace tube via a transfer tube that was 4 mm in inner diameter and 0.8 m in length, which was heated at a temperature within the range of 323–343 K. The relative humidity of the gas was measured in the temperature-controlled anterior chamber connected to the furnace tube. The relative humidity obtained from these measurements was used as the feedback signal for PID controls for the flow rates of dry N_2 and wet N_2 in order to control the $p(H_2O)$ of the mixed gas. Accordingly, $p(H_2O)$ was set to be a constant value within the range of 0.14–7.63 kPa as a function of the relative humidity and the temperature of the anterior chamber.

Figure S1 shows an example of the TG measurement for the $Ca(OH)_2$ sample under controlled $p(H_2O)$ conditions. Prior to set the sample in the instrument, the temperatures of the circulating water, the water bath in the humidity controller, and the transfer tube between the humidity controller and the TG–DTA instrument were stabilized at predetermined values. After setting the control value of the relative humidity of the flowing gas to zero, dry N_2 gas (400 cm^3 min^{-1}) was introduced into the TG–DTA instrument from the front of the reaction tube via the humidity controller and the transfer tube. At the same time, a purge with dry N_2 was also introduced from the back of the balance system and pushed toward the reaction tube at a rate of 50 cm^3 min^{-1}. These gases were discharged from the gas line positioned at the end of the reaction tube near the joint part of the reaction tube and the balance system. The relative humidity of the flowing gas was continuously measured in the anterior chamber connected to the front of the reaction tube, together with the temperature of the anterior chamber, in order to calculate the $p(H_2O)$ value for the flowing gas. After the sample was placed in the TG–DTA instrument, it was heated to a predetermined temperature (T_1) at $\beta = 5$ K min^{-1} in a stream of dry N_2 gas. As soon as the sample temperature reached the desired T_1, the relative humidity was switched to a programed value (H_1) for the TG measurement. The sample was kept at T_1 for 30 min in order to ensure stability in the system. Subsequently, the sample was heated according to the temperature program of nonisothermal or isothermal measurement in a stream of wet N_2 gas (400 cm^3 min^{-1}) under the controlled $p(H_2O)$ conditions. After the temperature program for the TG measurement was completed, the relative humidity in the system was immediately switched to zero. The reaction tube was cooled at $\beta = -10$ K min^{-1} in a stream of dry N_2 gas (400 cm^3 min^{-1}) in order to avoid possible condensation of water vapor.

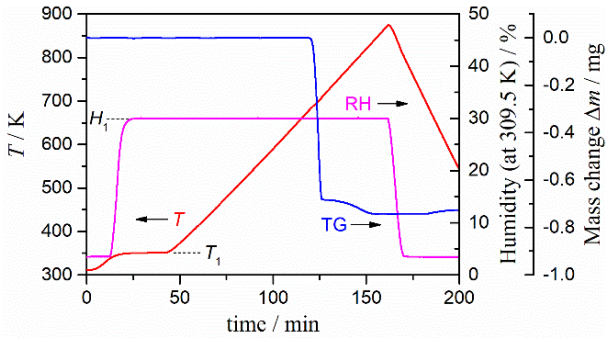

Figure S1. An example of the TG measurement obtained for the $Ca(OH)_2$ sample (m_0 = 3.002 mg) as recorded at $\beta = 5$ K min^{-1} in a stream of wet N_2 gas (400 cm^3 min^{-1}) by controlling the relative humidity at 30% at 309.5 K.

S2. Sample characterization

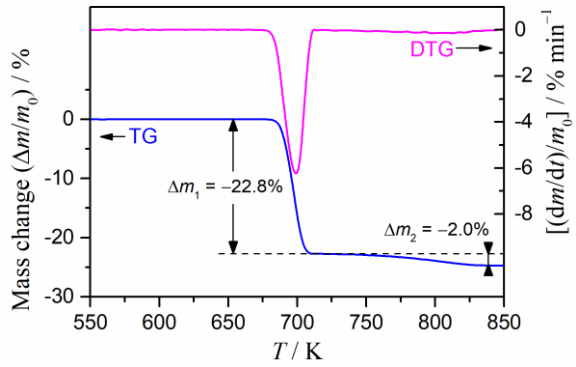

Figure S2. Typical TG–DTG curves for the $Ca(OH)_2$ sample (m_0 = 3.002 mg) as recorded at β = 5 K min^{-1} in a stream of wet N_2 gas (400 cm^3 min^{-1}) with $p(H_2O)$ = 1.81 kPa.

S3. Kinetics of the induction period

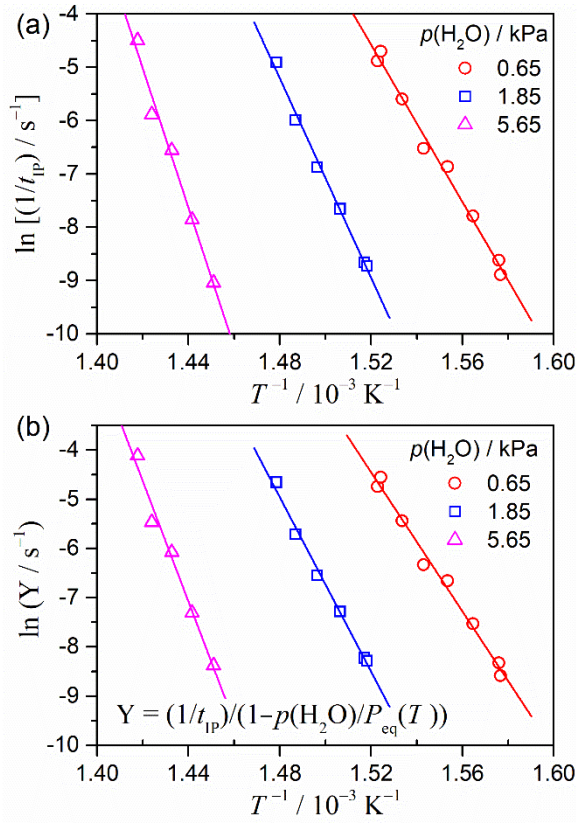

Figure S3. Arrhenius-type plots for the IP of the thermal decomposition of $Ca(OH)_2$ at different temperatures under various $p(H_2O)$ conditions: (a) conventional Arrhenius plot and (b) modified Arrhenius plot with the accommodation function of eqn (10).

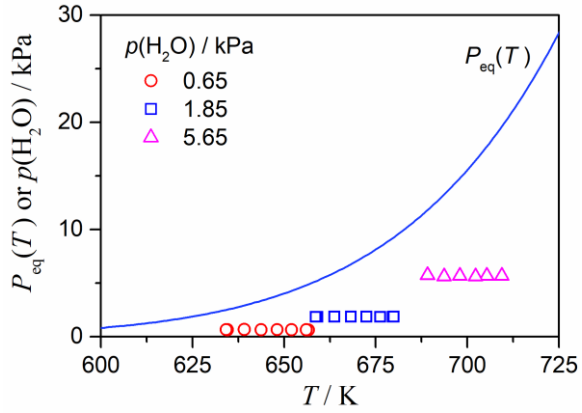

Figure S4. Equilibrium water vapor pressure, $P_{eq}(T)$, for the reversible reaction of eqn (6), together with the (T, $p(H_2O)$) values for the mass-loss measurements under isothermal conditions.

Table S1. Kinetic parameters for the IP process, as determined according to the conventional Arrhenius plot based on eqn (8) and the modified Arrhenius plot based on eqn (11) with the accommodation function of eqn (10)

Equation	$a(p(H_2O), P_{eq}(T))$	$p(H_2O)$ / kPa	$E_{a,IP}$ / kJ mol^{-1}	ln[$A_{IP}f(\alpha_{IP})$ / s^{-1}]	$-\gamma^a$
eqn (8)	———	0.65 ± 0.1	612.5 ± 24.3	107.4 ± 4.6	0.9953
		1.85 ± 0.1	778.0 ± 30.5	133.3 ± 5.5	0.9969
		5.65 ± 0.5	1085.6 ± 78.7	180.4 ± 13.6	0.9922
eqn (11)	eqn (10)	0.65 ± 0.1	587.5 ± 24.1	103.0 ± 4.5	0.9950
		1.85 ± 0.1	737.0 ± 31.5	126.2 ± 5.7	0.9963
		5.65 ± 0.5	1016.9 ± 80.6	169.1 ± 13.9	0.9907

[a] Correlation coefficient of the linear regression analysis.

S4. Kinetics of the mass-loss process

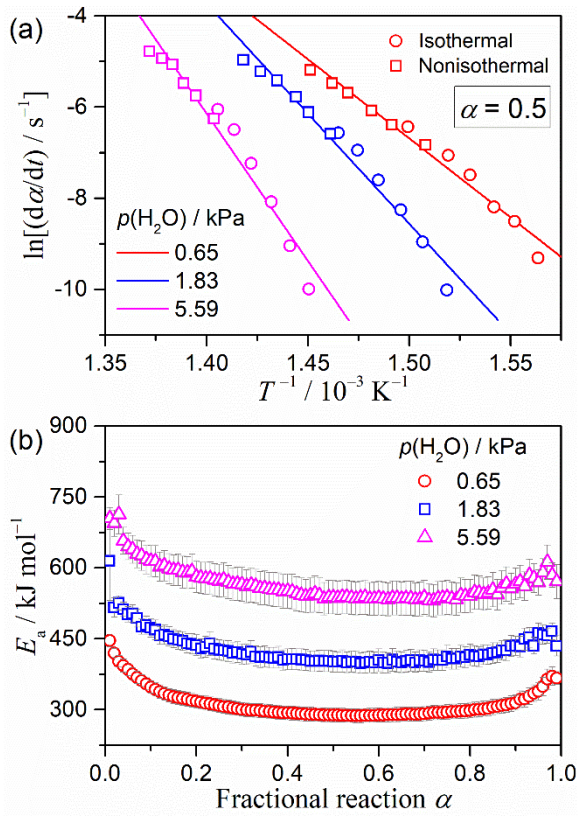

Figure S5. Results of the conventional Friedman plots as applied to the mass-loss process of the thermal decomposition of $Ca(OH)_2$ under isothermal and linear nonisothermal conditions in various $p(H_2O)$ conditions: (a) Friedman plots at α = 0.5 and (b) E_a values at different α.

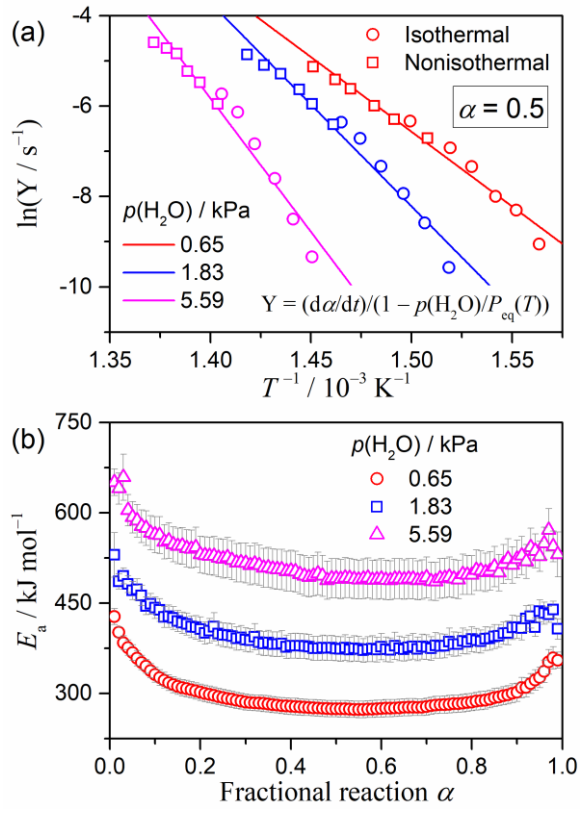

Figure S6. Results of the modified Friedman plots with the accommodation function of eqn (10) as applied to the mass-loss process of the thermal decomposition of $Ca(OH)_2$ under isothermal and linear nonisothermal conditions in different $p(H_2O)$ conditions: (a) modified Friedman plots at α = 0.5 and (b) E_a values at different α.

S5. Kinetic modeling of the consecutive IP–SR–PBR process under different water vapor pressures

Table S2. Kinetic equations for the IP–SR–PBR(n) model

n	$\frac{d\alpha}{dt} =$
1	a) $t - t_{IP} \le 1/k_{PBR(1)}$: $$k_{PBR(1)}\left[1-\exp\left(-k_{SR}\left(t-\frac{1}{k_{IP}}\right)\right)\right]$$ b) $t - t_{IP} \ge 1/k_{PBR(1)}$: $$k_{PBR(1)}\exp\left(-k_{SR}\left(t-\frac{1}{k_{IP}}\right)\right)\left[\exp\left(\frac{k_{SR}}{k_{PBR(1)}}\right)-1\right]$$
2	a) $t - t_{IP} \le 1/k_{PBR(2)}$: $$-2k_{PBR(2)}\left[\left(1+\frac{k_{PBR(2)}}{k_{SR}}\right)\exp\left(-k_{SR}\left(t-\frac{1}{k_{IP}}\right)\right)+k_{PBR(2)}\left(t-\frac{1}{k_{IP}}\right)-\left(1+\frac{k_{PBR(2)}}{k_{SR}}\right)\right]$$ b) $t - t_{IP} \ge 1/k_{PBR(2)}$: $$-2k_{PBR(2)}\exp\left(-k_{SR}\left(t-\frac{1}{k_{IP}}\right)\right)\left[1+\frac{k_{PBR(2)}}{k_{SR}}-\frac{k_{PBR(2)}}{k_{SR}}\exp\left(\frac{k_{SR}}{k_{PBR(2)}}\right)\right]$$
3	a) $t - t_{IP} \le 1/k_{PBR(3)}$: $$-3k_{PBR(3)}\left[\left(1+2\frac{k_{PBR(3)}}{k_{SR}}+2\left(\frac{k_{PBR(3)}}{k_{SR}}\right)^2\right)\exp\left(-k_{SR}\left(t-\frac{1}{k_{IP}}\right)\right)-\left(-k_{PBR(3)}\left(t-\frac{1}{k_{IP}}\right)\right)^2+2k_{PBR(3)}\left(\frac{k_{PBR(3)}}{k_{SR}}+1\right)\left(t-\frac{1}{k_{IP}}\right)-\left(1+2\frac{k_{PBR(3)}}{k_{SR}}+2\left(\frac{k_{PBR(3)}}{k_{SR}}\right)^2\right)\right]$$ b) $t - t_{IP} \ge 1/k_{PBR(3)}$: $$3k_{PBR(3)}\exp\left(-k_{SR}\left(t-\frac{1}{k_{IP}}\right)\right)\left[2\left(\frac{k_{PBR(3)}}{k_{SR}}\right)^2\left(\exp\left(\frac{k_{SR}}{k_{PBR(3)}}\right)-1\right)-\left(1+2\frac{k_{PBR(3)}}{k_{SR}}\right)\right]$$

Table S3. Optimized rate constants for the consecutive reaction steps of IP, SR, and PBR(2) for the isothermal decomposition of $Ca(OH)_2$ at different temperatures under different $p(H_2O)$ conditions.

$p(H_2O)$ / kPa	T / K	k_{IP} / s^{-1}	k_{SR} / s^{-1}	$k_{PBR(2)}$ / s^{-1}	$r^{2,a}$	
					differential	integral
0.65 ± 0.01	634.5	1.38×10^{-4}	1.16×10^{-4}	3.46×10^{-5}	0.9726	0.9950
	639.5	4.14×10^{-4}	2.14×10^{-4}	1.01×10^{-4}	0.9985	0.9998
	644.1	1.04×10^{-3}	5.37×10^{-4}	2.24×10^{-4}	0.9987	0.9999
	648.1	1.47×10^{-3}	6.75×10^{-3}	3.22×10^{-4}	0.9981	0.9999
	653.1	3.70×10^{-3}	1.39×10^{-3}	7.06×10^{-4}	0.9950	0.9997
	657.9	9.12×10^{-3}	5.02×10^{-3}	6.26×10^{-4}	0.9968	0.9998
1.85 ± 0.01	658.4	1.62×10^{-4}	1.18×10^{-4}	4.37×10^{-5}	0.9946	0.9999
	663.4	4.72×10^{-4}	2.74×10^{-4}	1.15×10^{-4}	0.9946	0.9999
	668.2	1.04×10^{-3}	6.01×10^{-4}	2.79×10^{-4}	0.9954	0.9999
	673.1	2.49×10^{-3}	1.21×10^{-3}	5.92×10^{-4}	0.9983	0.9999
	678.0	7.40×10^{-3}	3.01×10^{-3}	7.69×10^{-4}	0.9893	0.9994
	682.7	3.70×10^{-2}	4.88×10^{-3}	1.23×10^{-3}	0.9979	0.9999
5.65 ± 0.04	688.9	1.18×10^{-4}	1.00×10^{-4}	3.79×10^{-5}	0.9779	0.9991
	693.8	3.85×10^{-4}	2.76×10^{-4}	1.12×10^{-4}	0.9924	0.9997
	698.5	1.42×10^{-3}	7.27×10^{-4}	3.20×10^{-4}	0.9954	0.9998
	703.3	2.78×10^{-3}	1.61×10^{-3}	7.15×10^{-4}	0.9904	0.9993
	707.5	6.21×10^{-3}	4.74×10^{-3}	1.28×10^{-3}	0.9919	0.9997
	712.2	1.80×10^{-2}	9.28×10^{-3}	1.87×10^{-3}	0.9901	0.9996

[a] Determination coefficient of the nonlinear least-squares analysis.

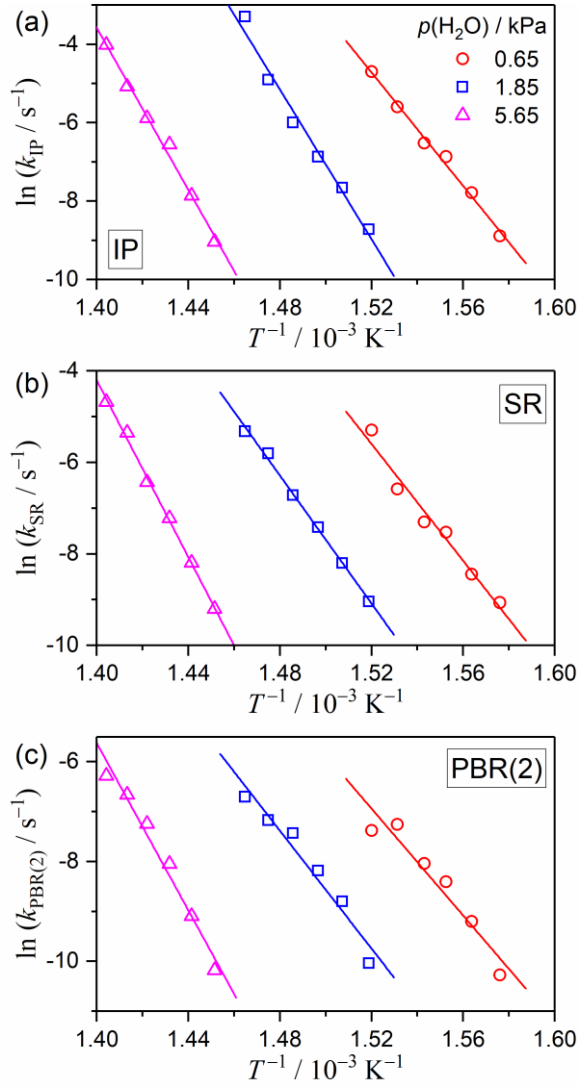

Figure S7. Conventional Arrhenius plots that describe the temperature dependences of the rate constants for the IP, SR, and PBR(2) steps in the thermal decomposition of $Ca(OH)_2$ under various $p(H_2O)$ conditions: (a) IP, (b) SR, and (c) PBR(2).

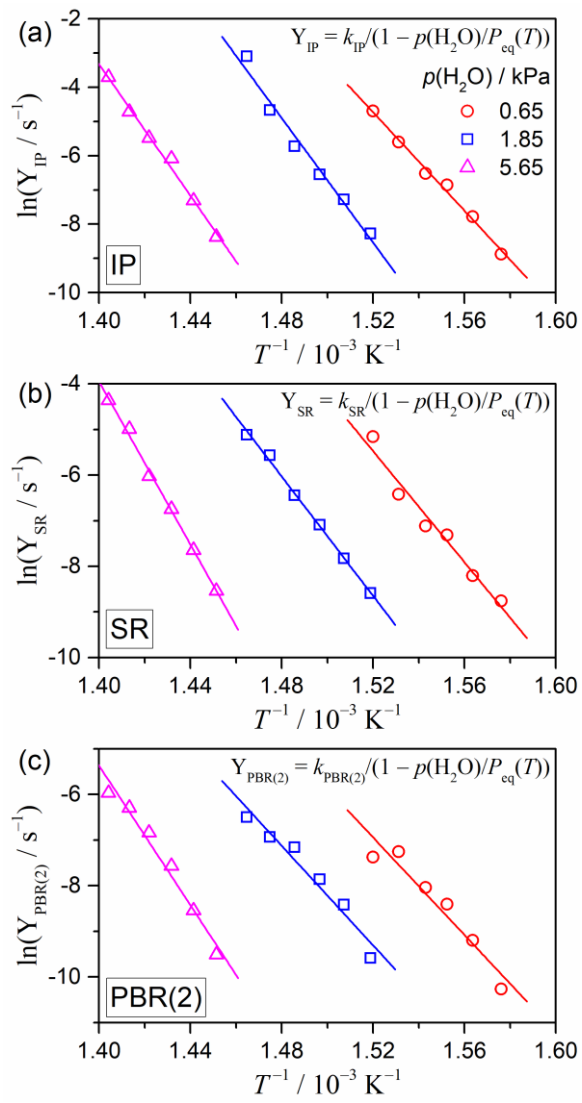

Figure S8. Modified Arrhenius plots with the accommodation function of eqn (10), which describe the temperature dependences of the corrected rate constants for the IP, SR, and PBR(2) steps in the thermal decomposition of $Ca(OH)_2$ under various $p(H_2O)$ conditions: (a) IP, (b) SR, and (c) PBR(2).

Table S4. Arrhenius parameters for each reaction step under a particular $p(H_2O)$ value, as determined according to a conventional Arrhenius plot based on eqn (24) and a modified Arrhenius plot based on eqn (25) with the accommodation function of eqn (10)

Equation	$a(p(H_2O), P_{eq}(T))$	Reaction step	$p(H_2O)$ / kPa	E_a / kJ mol^{-1}	ln(A / s^{-1})	$-\gamma$[a]
eqn (24)	———	IP	0.65 ± 0.1	600.2 ± 26.4	105.0 ± 5.0	0.9961
			1.85 ± 0.1	794.1 ± 54.7	136.2 ± 9.9	0.9906
			5.65 ± 0.5	859.5 ± 37.8	141.1 ± 6.5	0.9961
		SR	0.65 ± 0.1	530.6 ± 45.6	91.4 ± 8.5	0.9855
			1.85 ± 0.1	581.5 ± 15.7	97.2 ± 2.9	0.9985
			5.65 ± 0.5	803.6 ± 20.8	131.1 ± 3.6	0.9986
		PBR(2)	0.65 ± 0.1	445.1 ± 62.0	74.4 ± 11.6	0.9633
			1.85 ± 0.1	491.0 ± 53.4	80.0 ± 9.6	0.9771
			5.65 ± 0.5	696.6 ± 54.6	111.7 ± 9.4	0.9879
eqn (25)	eqn (10)	IP	0.65 ± 0.1	597.8 ± 26.2	104.6 ± 4.9	0.9961
			1.85 ± 0.1	756.4 ± 56.7	129.8 ± 10.2	0.9889
			5.65 ± 0.5	799.0 ± 35.3	131.2 ± 6.1	0.9961
		SR	0.65 ± 0.1	506.0 ± 46.7	87.0 ± 8.7	0.9834
			1.85 ± 0.1	543.8 ± 14.9	90.8 ± 2.7	0.9985
			5.65 ± 0.5	743.1 ± 20.5	121.2 ± 3.5	0.9985
		PBR(2)	0.65 ± 0.1	444.1 ± 61.8	74.3 ± 11.6	0.9633
			1.85 ± 0.1	453.3 ± 51.0	73.6 ± 9.2	0.9756
			5.65 ± 0.5	636.1 ± 50.0	101.7 ± 8.6	0.9878

[a] Correlation coefficient of the linear regression analysis.